Using Remote Control Aerial Vehicles to Study Variability of Airborne Particulates

Authors: Harrison, William A., Lary, David J., Nathan, Brian J., and Moore, Alec G.

Source: Air, Soil and Water Research, 8(1)

Published By: SAGE Publishing

URL: https://doi.org/10.1177/ASWR.S30774

Using Remote Control Aerial Vehicles to Study Variability of Airborne Particulates

William A. Harrison, David J. Lary, Brian J. Nathan and Alec G. Moore

William B. Hanson Center for Space Sciences, University of Texas at Dallas, TX, USA.

ABSTRACT: Airborne particulates play a significant role in the atmospheric radiative balance and impact human health. To characterize this impact, global-scale observations and data products are needed. Satellite products allow for this global coverage but require in situ validations. This study used a remote-controlled aerial vehicle to look at the horizontal, vertical, and temporal variability of airborne particulates within the first 150 m of the atmosphere. Four flights were conducted on December 4, 2014, between 12:00 pm and 5:00 pm local time. The first three flights flew a pattern of increasing altitude up to 140 m. The fourth flight was conducted at a near-constant altitude of 60 m. The mean $PM_{2.5}$ concentration for the three flights with varying altitude was 36.3 $\mu g/m^3$, with the highest concentration occurring below 10 m altitude. The overall vertical variation was very small with a standard deviation of only 3.6 $\mu g/m^3$. $PM_{2.5}$ concentration also did not change much throughout the day with mean concentrations for the altitude-varying flights of 35.1, 37.2, and 36.8 $\mu g/m^3$. The fourth flight, flown at a near-constant altitude, had a lower concentration of 23.5 $\mu g/m^3$.

KEYWORDS: $PM_{2.5}$, vertical variability, UAV, air quality

CITATION: Harrison et al. Using Remote Control Aerial Vehicles to Study Variability of Airborne Particulates. *Air, Soil and Water Research* 2015:8 43–51 doi:10.4137/ASWR.S30774.

TYPE: Original Research

RECEIVED: June 17, 2015. **RESUBMITTED:** July 30, 2015. **ACCEPTED FOR PUBLICATION:** August 4, 2015.

ACADEMIC EDITOR: Carlos Alberto Martinez-Huitle, Editor in Chief

PEER REVIEW: Three peer reviewers contributed to the peer review report. Reviewers' reports totaled 1,377 words, excluding any confidential comments to the academic editor.

FUNDING: The authors greatly appreciate the support of NASA with research funding through award NNX11AL18G. The authors confirm that the funder had no influence over the study design, content of the article, or selection of this journal.

COMPETING INTERESTS: Authors disclose no potential conflicts of interest.

CORRESPONDENCE: wah091020@utdallas.edu

Paper subject to independent expert blind peer review. All editorial decisions made by independent academic editor. Upon submission manuscript was subject to anti-plagiarism scanning. Prior to publication all authors have given signed confirmation of agreement to article publication and compliance with all applicable ethical and legal requirements, including the accuracy of author and contributor information, disclosure of competing interests and funding sources, compliance with ethical requirements relating to human and animal study participants, and compliance with any copyright requirements of third parties. This journal is a member of the Committee on Publication Ethics (COPE).

Published by Libertas Academica. Learn more about this journal.

Introduction

Airborne particulates play a significant role in our everyday lives. This includes the role of the particulates in the radiative balance of the atmosphere[1–6] and their effect on human health.[7–16] These issues can be due to long-term exposure, such as lung cancer and cardiopulmonary disease,[11–13] or short-term exposure, such as respiratory problems and bacterial infections.[7,14–16]

To fully characterize all the roles airborne particulates play in our lives on a global scale, direct observations are needed. Satellite-based data products allow for full global coverage on a daily basis, but the data need in situ validation. Conventional ground-based air quality monitoring stations do not provide data on an appropriate spatial scale for this validation.[17] Validation with traditional aerial vehicles can be challenging in the lowermost atmospheric boundary layer due to flight safety considerations. Previous studies have looked at air quality variability using conventional aircrafts.[18–24] For safety reasons, the measurements are restricted to the upper levels of the boundary layer and above. Data gathered in the lower layers of the boundary layer are critical for validating satellite-based observations and data products due to the high abundance of aerosols in the boundary layer and the presence of sharp vertical gradients. Comprehensive sampling of the full aerosol size distribution and profiling of the lowermost boundary layer are rare.

Several studies have used tethered balloons to study airborne particulates.[25–28] These studies have either taken measurements at a set location across changing altitudes,[25,26] providing information on temporal and vertical variation but not horizontal, or at set locations and set altitudes,[27,28] only providing information on temporal variation. This study provides data on all three variations: vertical, horizontal, and temporal.

The motivation for this study was to prepare a validation platform for the upcoming National Aeronautics and Space Administration (NASA) missions, including the NASA Aerosol-Cloud-Ecosystems and Pre-Aerosol, Clouds, and ocean Ecosystem missions.[29] This study uses a remote-controlled aerial vehicle to look at the horizontal, vertical, and temporal variability of airborne particulates within the first 150 m of the atmosphere. This platform, due to its size and maneuverability, is uniquely qualified to gather the much needed data in this lower level of the boundary layer. To the best of our knowledge, this is the first time a zero-emission aerial vehicle has been used to quantify the aerosol size distribution and its vertical, horizontal, and temporal variation. Thus, this study sets the stage for the next generation of satellite validation methodologies.

Instrumentation

A large remote-controlled model airplane was built from an AMR Payload Master 100 kit. This kit was modified to use twin-electric motors mounted on the wings allowing for sample collection in undisturbed air from the nose of the aircraft. It was also modified to use a tricycle-style landing gear, instead of a tail wheel–style gear, to support the increased nose weight

of the sensor package. This vehicle was originally built and flown during a methane gas measurement campaign conducted in October 2013, where it successfully completed 34 flights.

For this aerial measurement campaign, the plane needed to be able to fly a precise path at specific altitudes, and then repeat the exact flight plan multiple times over multiple days. To accomplish this, a MicroPilot MP2128LRC autopilot system was employed. The autopilot is capable of flying a complete mission from takeoff to landing with way-points set in GPS coordinates, including altitude and airspeed. This system incorporates three 3-axis gyroscopes/accelerometers, GPS, pressure altimeter, and pressure airspeed sensor onto a single circuit board.[30] For communication with the ground station laptop, a Microhard 900-mHz radio modem was installed on the vehicle.

To monitor particulates, a sensor package was built and installed in the twin-engine remote-controlled airplane. The package utilized a Grimm 1109 aerosol spectrometer mounted in the nose of the plane. An intake probe was mounted in the cowl to allow samples to be collected in clean, undisturbed air.

A Raspberry Pi model B+ microcomputer was used to record data from temperature, pressure, humidity, and airspeed sensors. A digital compass and GPS modules were used to calculate wind speed and direction. The GPS antennas for both the sensor package and the autopilot system were installed just behind the main wing.

A touch-screen LCD panel was installed in the front window of the airplane to display data from the Raspberry Pi sensor package. This allowed for verification of data collection from the sensor package prior to takeoff and to stop data collection after landing.

Data Collection

Four flights were conducted on December 4, 2014, starting at 12:00 pm and ending at 5:00 pm local time. Each flight lasted from 6 to 8 minutes and consisted of an oval pattern with vertices of approximately 650 m by 250 m flying at an average airspeed of 60 knots. During the first three flights, the altitude was increased after each lap, starting at approximately 30 m, in 15-m intervals up to 140 m. The fourth flight was conducted at a near-constant altitude of 60 m.

Wind speed and direction were calculated after all flights were completed by using the heading and airspeed vector and the ground speed and ground track vector. Due to differences in data collection rates between the GPS sensor and the airspeed/compass combination, the wind speed and direction were only calculated for straight path portions of the flight. Straight path was defined as portions of the flight where heading and ground track differed by less than 10°. Portions of the flight not within this limit were assumed to have a wind speed and direction equal to the mean from the previous straight path segment.

Discussion

Let us start by considering the vertical structure of the mean PM concentration in the lowest part of the boundary layer. Data from each flight were averaged into 10-m increments between the ground and 140 m. The mean $PM_{2.5}$ concentration for the first three flights was 36.3 ± 3.6 µg/m^3. The small deviations suggest a very well mixed boundary layer. Figure 1 shows the summary vertical profiles for the first three flights. All three size fractions showed the highest PM concentration below 10 m. For $PM_{2.5}$, the highest concentration occurred at

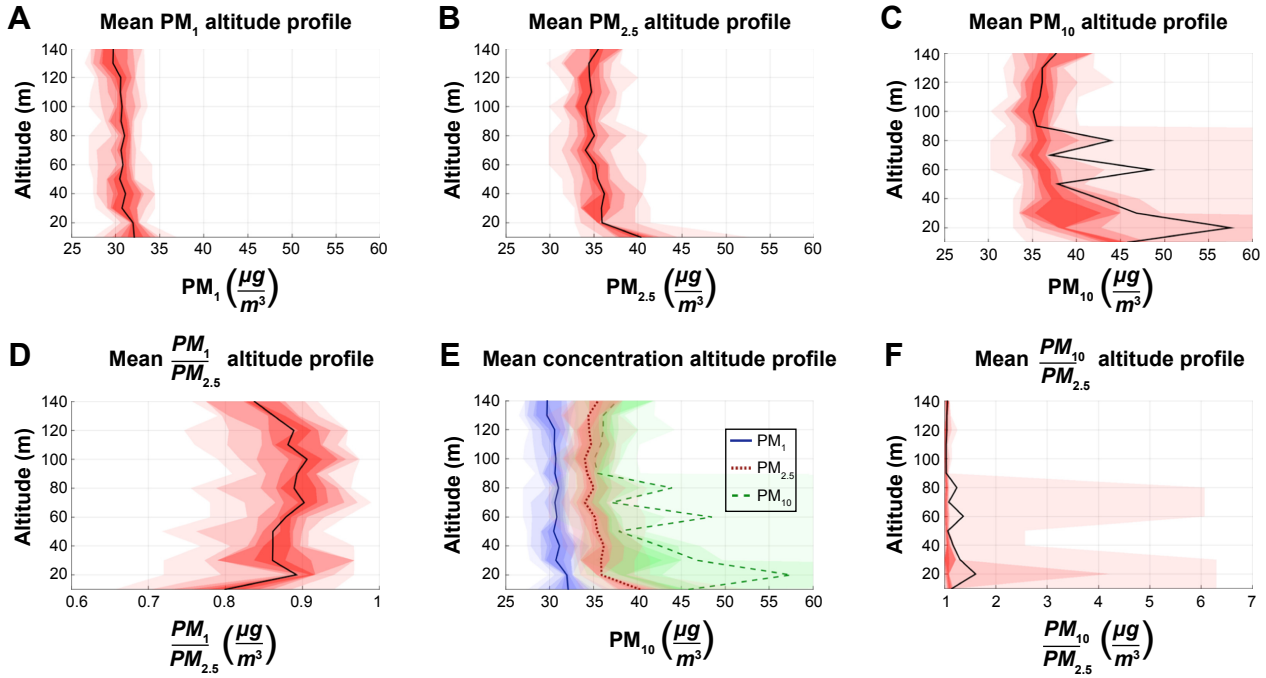

Figure 1. Mean concentrations of PM_1 (panel **A**), $PM_{2.5}$ (panel **B**), and PM_{10} (panel **C**) as a function of altitude for the first three flights. Panels **D**–**F** are a comparison of PM_1 and PM_{10} concentrations to $PM_{2.5}$ concentrations for the first three flight.

9.1 m. Above 10 m, the mean $PM_{2.5}$ concentration was only 34.8 ± 2.2 μg/m^3, while below 10 m the mean concentration was 40.3 ± 3.5 μg/m^3. The PM_1 concentration was the most consistent, with a standard deviation of 2.0 μg/m^3, while the $PM_{2.5}$ concentration had a standard deviation of 3.6 μg/m^3 and PM_{10} concentration had a standard deviation of 21.3 μg/m^3.

A key issue addressed in this paper is the characterization of aerosol variability: horizontal, vertical, and temporal. The plots in Figure 1 are the summary of many measurements, so the full PDF of aerosol distributions at each altitude is depicted by using shading to showcase the different percentiles (0%, 10%, 20%,… 100%). The overlaid line is the mean value.

The profiles show the summary value for different size fractions PM_1 (panel A), $PM_{2.5}$ (panel B), and PM_{10} (panel C). To characterize the relative abundance of these size fractions, the ratios of $PM_1/PM_{2.5}$ (panel D) and $PM_{10}/PM_{2.5}$ (panel F) are shown. Note that the $PM_1/PM_{2.5}$ ratio is less than 1 in the sampling of the boundary layer, typically in the range of 0.7–0.95. The ratio $PM_{10}/PM_{2.5}$ (panel F) is typically larger than 1 in the range 1–6.

Temporal variation. The first three flights had the highest observed $PM_{2.5}$ concentrations at 35.1 ± 3.5 μg/m^3, 37.2 ± 3.3 μg/m^3, and 36.8 ± 3.9 μg/m^3, respectively, while the fourth flight saw a reduction in concentration to 23.5 ± 2.9 μg/m^3, shown in Figure 2. The histogram color scale indicates the air quality according to guidelines set by the Environmental Protection Agency (EPA). Each of the four flights was separated by approximately 1.5 hours. Thus, the four distributions show how the $PM_{2.5}$ concentration changed over time. The maximum variation in mean concentration between the first three flights is only 2.2 μg/m^3. This is less than the standard deviation of any of the three flights. The fourth and final flight saw a significant reduction in concentration of 13.3 μg/m^3 from the previous flight. This reduction in concentration is much higher than the variation of any of the first three flights, which indicates that the reduction is not a result of the flight being conducted at a constant altitude. This flight concluded at sunset; therefore, the reduction is most likely due to the changing boundary layer height.

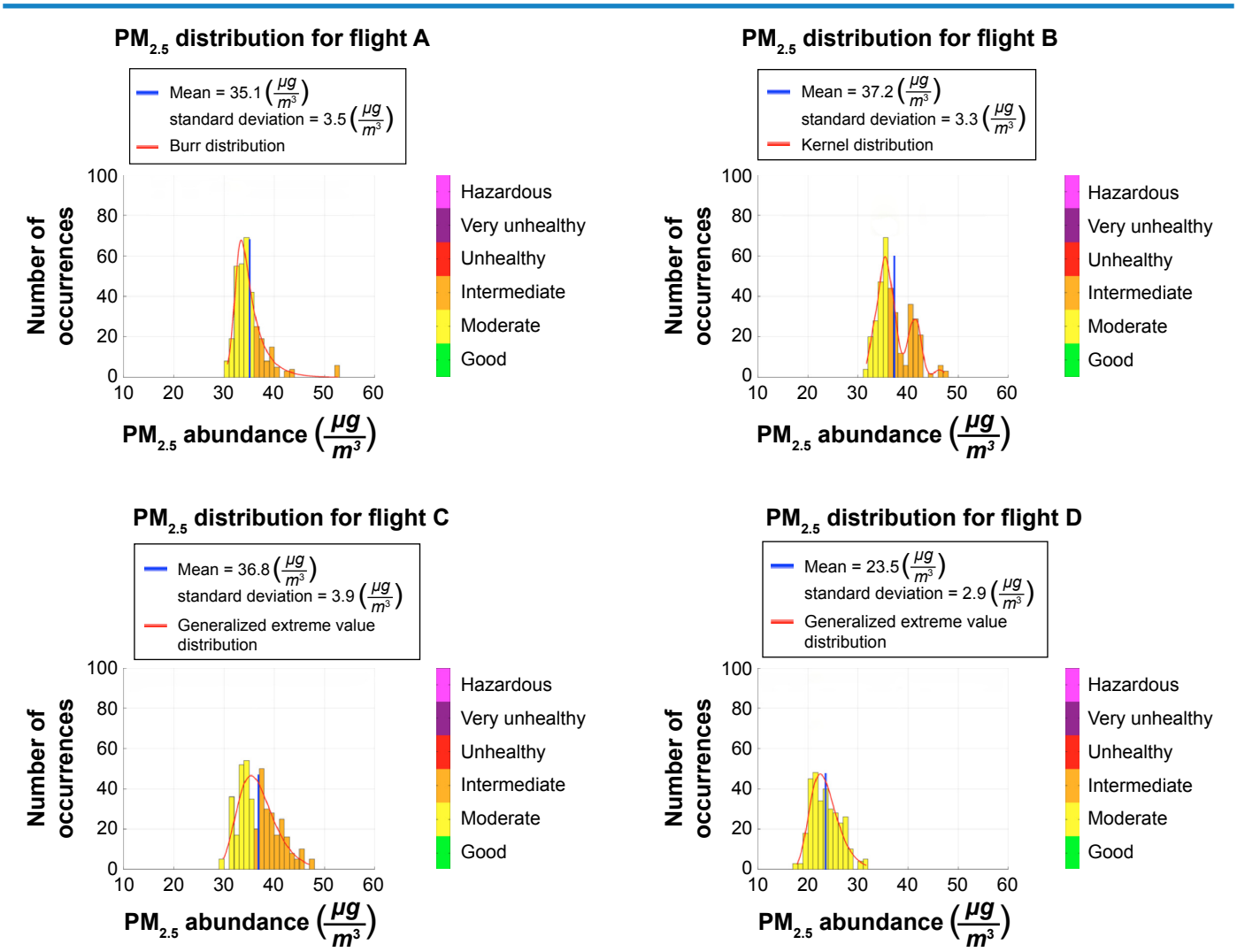

Figure 2. $PM_{2.5}$ distributions for each of the four flights. Color scale indicates the air quality using EPA standards.

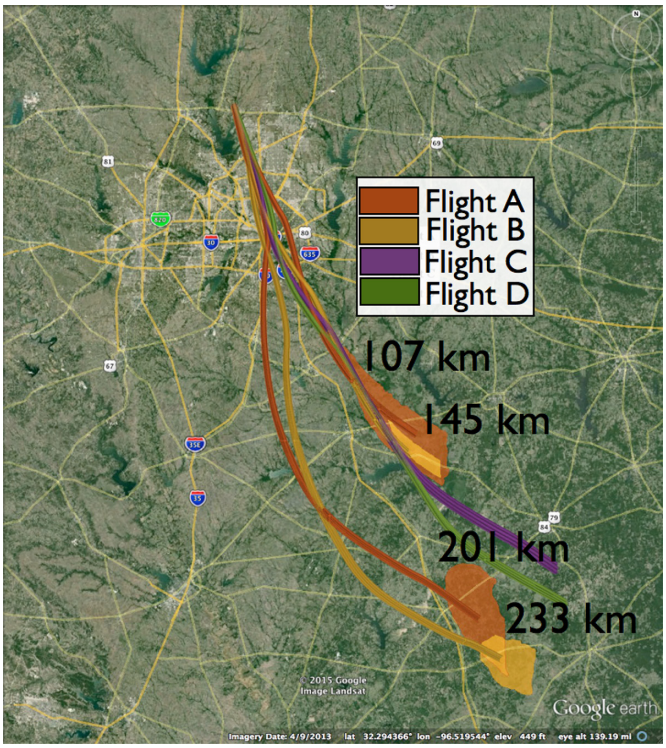

Figure 3. Map depicting air parcel trajectories for 24 hours prior to measurement for each of the four flights.

Air parcel origin. The temporal variation is in part due to where the air parcels originated. To examine the likely air parcel origin, the Hybrid Single Particle Lagrangian Integrated Trajectory Model (HYSPLIT) model[31] was used to calculate 24-hour back-trajectories for each flight. The trajectories were calculated at 5-m increments up to 140 m and checked for any altitudes that originated on the ground within the 24 hours prior to measurement. Only the first two flights (A and B) had air parcels observed at higher altitudes that originated on the ground. Figure 3 shows the trajectories and the $PM_{2.5}$ distribution for each of the four flights. The colored traces represent the path of an air parcel at a single altitude, while the corresponding colored area outlines the region on the ground that air parcels from any altitude originated from. The distance from the region of measurement is also indicated on the map. Particulates from these areas are carried along by the wind and affect the overall measured PM concentration.

Let us now compare Flight A, with multiple air parcel altitudes originating on the ground, and Flight C, with no air parcel altitudes originating on the ground. Flight D will be described separately due to its much lower PM concentration and because the flight plan was altered to fly at a near-constant altitude of 60 m.

The map for Flight A, Figure 4 (left), shows the air parcel trajectories over the 24-hour period prior to measurement.

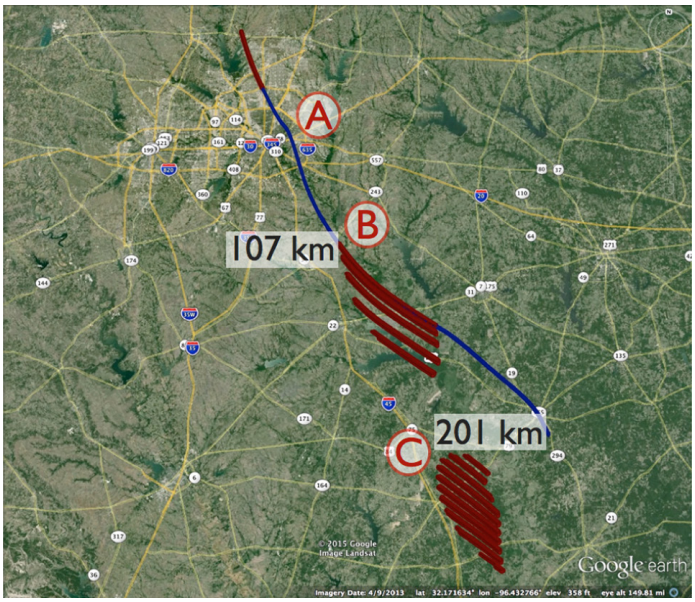

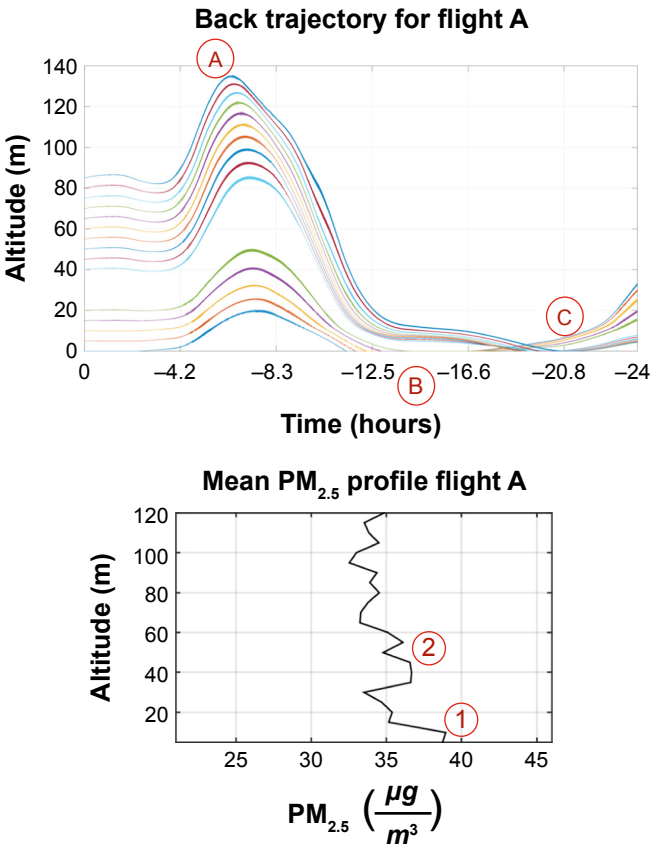

Figure 4. Map depicting air parcel trajectory over a 24-hour period prior to measurement of Flight A (left). Top right plot shows air parcel altitude as a function of time prior to measurement while the bottom right plot shows mean $PM_{2.5}$ concentration as a function of altitude.

The blue line, as an example, is the path of the air parcels measured at 0-m altitude. The blue line is colored red to indicate when this air parcel was close to the ground. Additional red marks on the map indicate where other air parcels, at varying altitudes, are closest to the ground. The plot in the upper right shows the altitude of air parcels over the prior 24 hours; only the altitudes for air parcels that originated on the ground are included in the plot. The 0 point on the *x*-axis is the measurement time. This shows how long before measurement the parcel was in contact with the ground, thus how long any particulates from that area had to settle out of the atmosphere. Note the specific points notated on the trajectory and corresponding notations on the map. Point A indicates the time and location of the highest altitude reached by each of the air parcels. Points B and C indicate the time and location of air parcels origin on the ground. The plot in the lower right shows how the mean $PM_{2.5}$ concentration changes with altitude. For this plot, measurements were averaged into 5-m-altitude bins. The highest measurements are observed in the lowest two bins, point 1, equating to 5 m and 10 m. There is a second peak occurring from 35 m to 60 m, point 2, which corresponds to a different section of air parcels that originated on the ground.

Figure 5 shows similar information for Flight C. In the map on the left, the only time where the air is close to the ground in the 24 hours prior to measurement (red area) is at the point of measurement in the northernmost tip of the trajectory, point A. This is reflected in the back-trajectory plot in the upper right were only one altitude is indicated. Points B and C on the trajectory, and reflected on the map, indicate the time and location of air parcel peak altitudes. The mean $PM_{2.5}$ concentration is still at its highest in the 5-m and 10-m bins, point 1, but there is not another peak until the 80-m mark, point 2. This sharp peak observed at a single altitude (80 m) is in contrast to the Flight A data, which shows an increased concentration along a range of altitudes (35–60 m).

Vertical variation. The largest PM concentrations are typically observed close to the ground. This study looks at how the concentration and particle size bin counts change with altitude. Figure 6 shows the altitude profile of PM_1, $PM_{2.5}$, and PM_{10} concentrations and particle size counts. In panels A and B, PM_1 and $PM_{2.5}$ concentrations both decrease above 40 m. Conversely, PM_{10} (panel C) has a strong concentration peak around 55 m, then returns to a fairly constant concentration above that. This peak may be a result of the low particle count. This is indicated by panel e, which shows particle count versus size for all altitude bins. For particle sizes above 3 microns, at most altitudes, the number of particles is less than 10 (the horizontal line). To see this more clearly, panels D, F, and G show particle count as a function of altitude for 0.25, 1, and 3 microns, respectively. The smaller particles have a much higher count, and larger variation, than the larger particles. However, with the much greater mass of the larger particles, a change in count of a few particles has a much greater effect on the overall concentration.

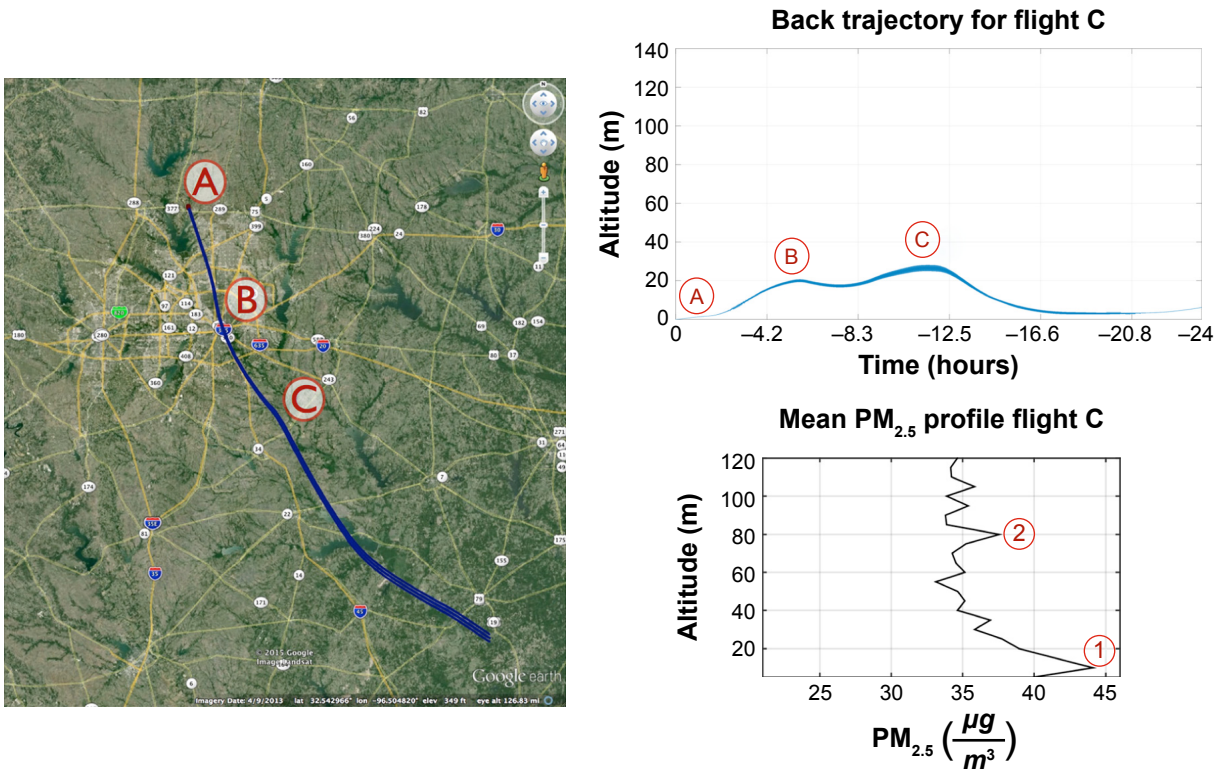

Figure 5. Map depicting air parcel trajectory over a 24-hour period prior to measurement of Flight C (left). Top right plot shows air parcel altitude as a function of time prior to measurement while the bottom right plot shows mean $PM_{2.5}$ concentration as a function of altitude.

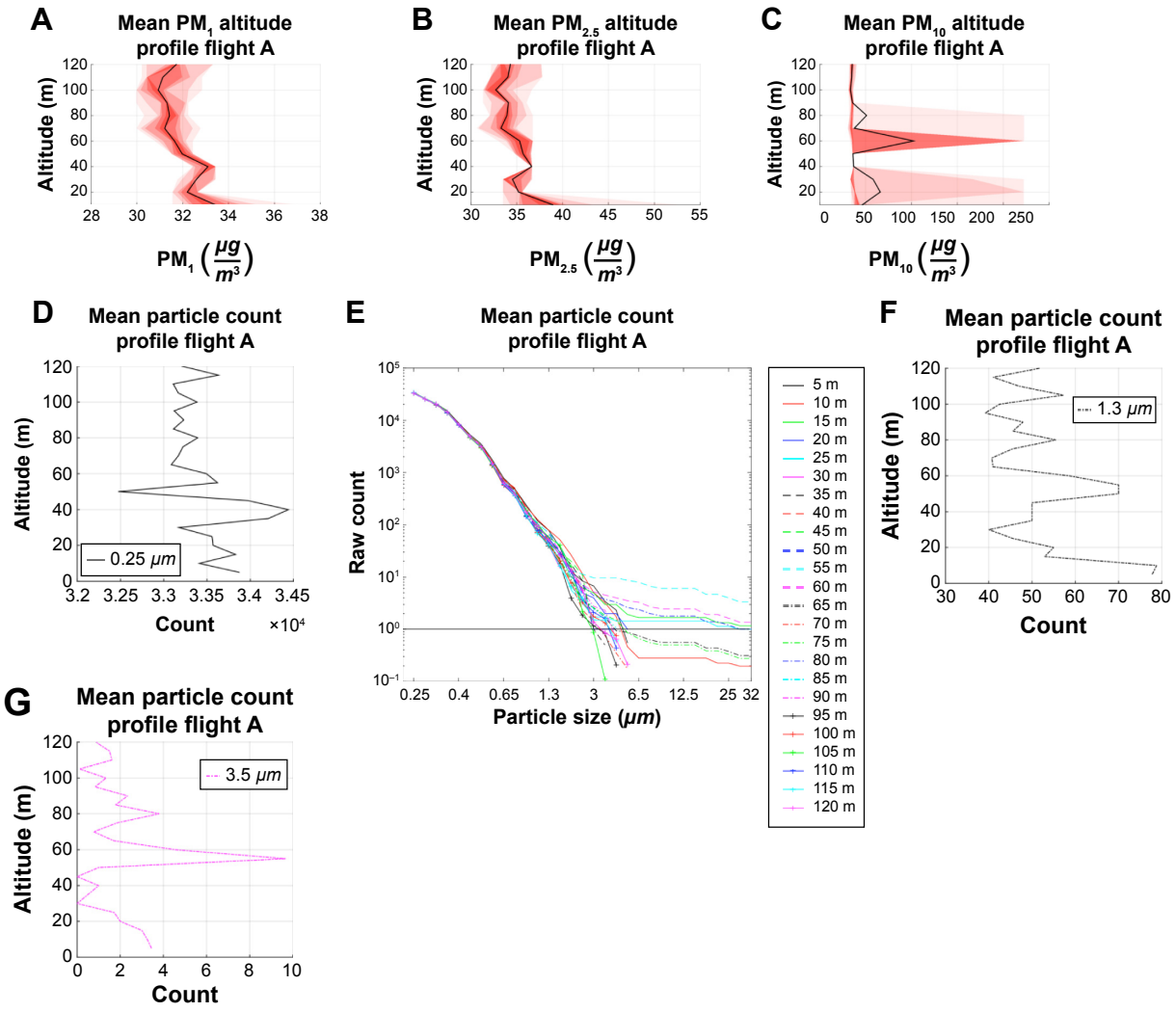

Figure 6. Flight A particle count profiles. Panels **A**, **B**, and **C** show mean concentration as a function of altitude for PM_1, $PM_{2.5}$, and PM_{10}, respectively. The shading indicates the measurement percentiles while the overlaid line is the mean value. Panel **E** shows particle count as a function of particle size for all altitude bins. Panels **D**, **F**, and **G** show particle count as a function of altitude for 0.25, 1.3, and 3.5 microns, respectively.

For Flight C, Figure 7 shows how particle count for all size bins, and specific sizes, changes with altitude. In this flight, panels A, B, and C show a decrease in concentration above 20 m, with a small peak at 80 m. A small peak is also seen in the particle count for the three size bins, around 80 m, in panels d, f, and g. For this flight, particle counts for the larger particles drop below 10 particles for all altitudes (panel E), whereas Figure 6 (panel E) showed a few altitudes where all size bins maintained more than 10 particles. This is an indication of the different sources of particulates. Recall the air parcel trajectories of Figures 4 and 5. For Flight A, air parcel at multiple higher altitudes originated on the ground away from the measurement site, whereas for Flight C, no higher altitude air parcel originated on the ground within 24 hours prior to measurement. Thus, larger particles were neither lifted to the higher altitudes nor had time to settle out of the atmosphere prior to measurement.

Horizontal variation. Satellite-based data products have finite resolution with a typical pixel size range of 250 m–10 km. Flight D was used to examine the horizontal variation at much finer scales across a pixel of satellite imagery. To minimize any variation caused by a change in altitude, this flight was conducted at a near-constant altitude of 60 m.

Figure 8 shows mean $PM_{2.5}$ concentration, standard deviation, and number of measurement points for the gridded measurement area. The top row is gridded into a 30 m × 15 m grid to show more detail in the horizontal variance. Note that most of the grid points only have one or two measurements per cell, thus the standard deviation for the majority of the flight is 0. This is not statistically significant as each cell only has a single data point. The bottom row is gridded into a 120 m × 65 m grid to increase the number of data points in each grid cell, allowing for a more robust statistical analysis. For this flight, mean concentration ranged from 20.5 to 24.9 $\mu g/m^3$ with a standard deviation range of 0.8–3.3 $\mu g/m^3$. This indicates that the horizontal variance for an area of this size is of the same order as the vertical variance (3.6 $\mu g/m^3$). The range

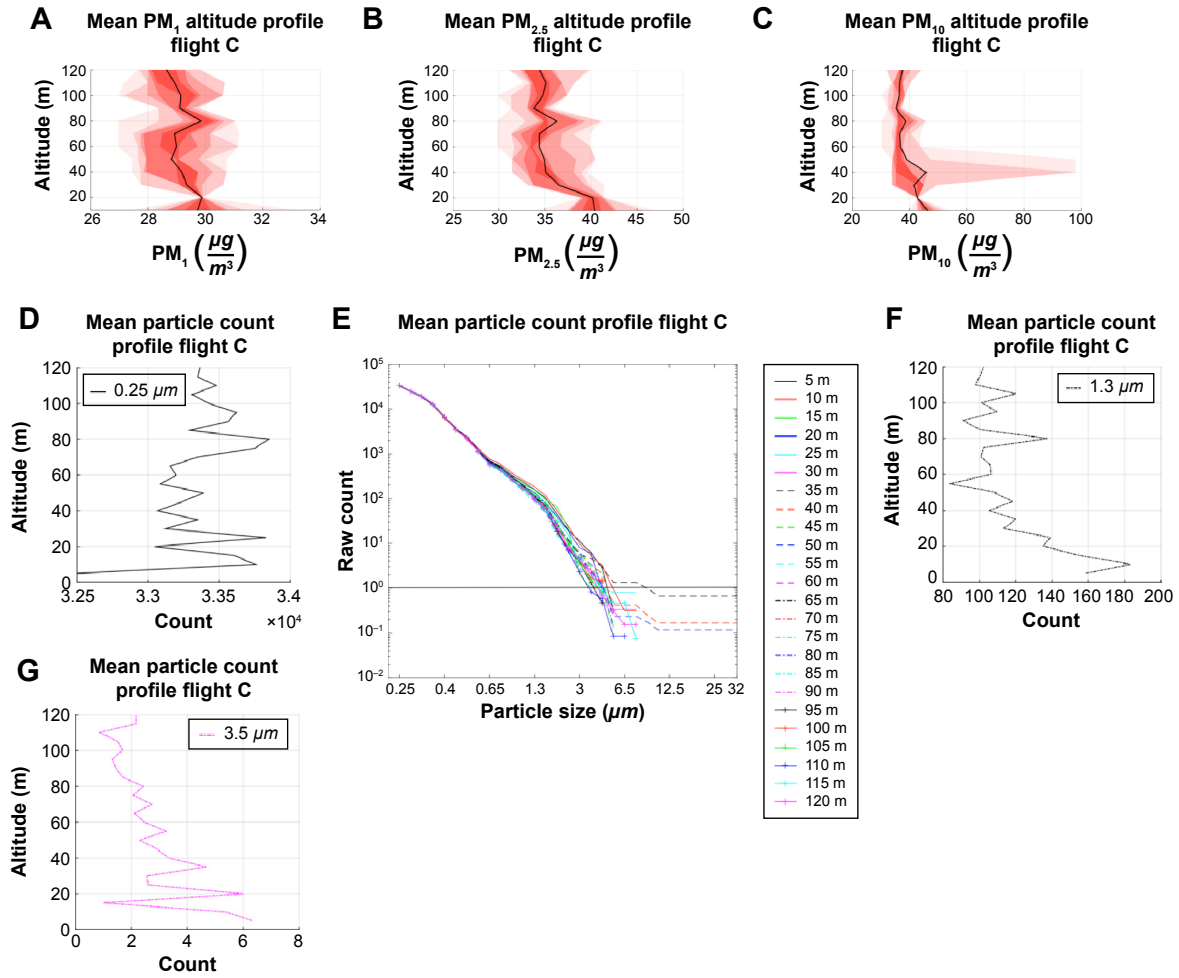

Figure 7. Flight C particle count profiles. Panels **A**, **B**, and **C** show mean concentration as a function of altitude for PM_1, $PM_{2.5}$, and PM_{10}, respectively. The shading indicates the measurement percentiles while the overlaid line is the mean value. Panel **E** shows particle count as a function of particle size for all altitude bins. Panels **D**, **F**, and **G** show particle count as a function of altitude for 0.25, 1.3, and 3.5 microns, respectively.

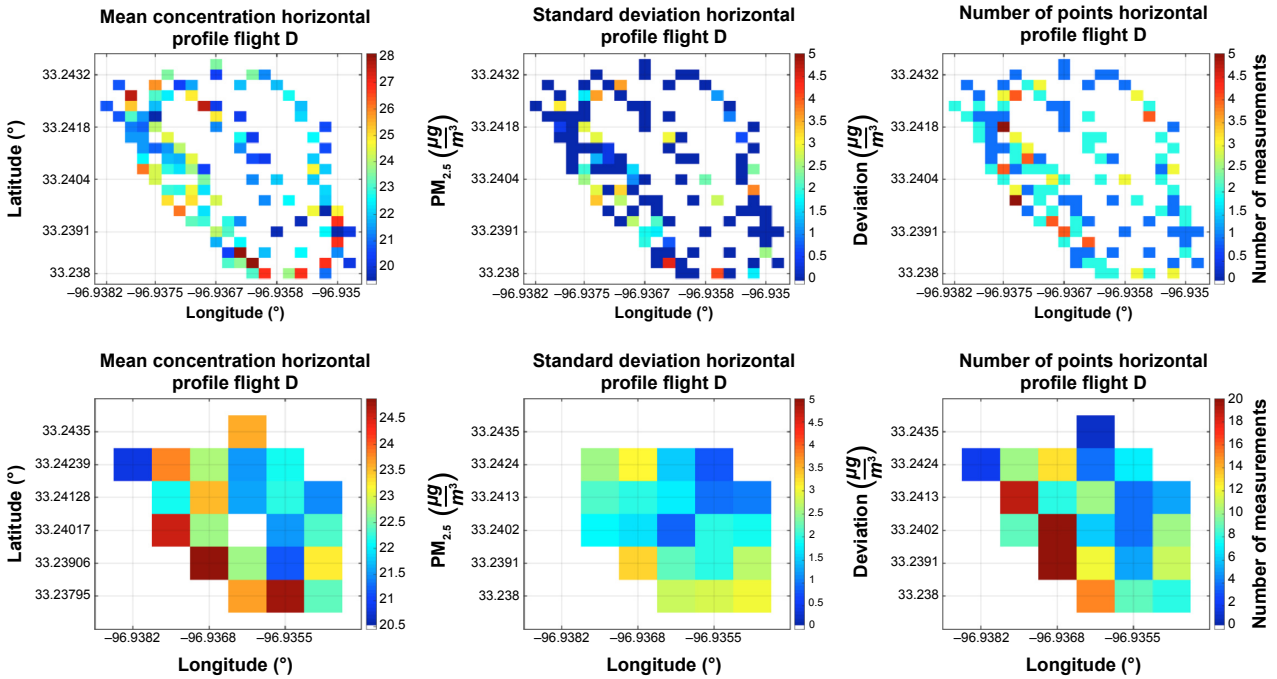

Figure 8. Mean $PM_{2.5}$ concentration, standard deviation, and number of measurements for Flight D divided into 30 m × 15 m (top) and 120 m × 65 m (bottom) grids.

of PM concentration or this area is approximately 4.4 μg/m^3 which is less than twice the highest standard deviation of any grid cell. This indicates that the variation across the entire area is similar to the variation of any given point of measurement. Thus, a data pixel of this size would still accurately characterize the concentration of the entire area. The variability could be larger for a larger or more diverse area as may be covered by satellite-based observations.

Conclusion

To the best of our knowledge, this is the first time a zero-emission aerial vehicle has been used to quantify the vertical, horizontal, and temporal variations of airborne particulates in the lower region of the boundary layer. Satellite-based data products may allow for full global coverage on a daily basis, but they need in situ validation. The platform used in this study is uniquely qualified for measurements in the all-important lower boundary layer, which are necessary for this validation. This study shows the value of this approach for the next generation of satellite validation methodology using aerial vehicles.

The mean $PM_{2.5}$ concentration for three flights with varying altitude was 36.3 μg/m^3, with the highest concentration occurring below 10 m altitude. The overall vertical variation was very small with a standard deviation of only 3.6 μg/m^3.

$PM_{2.5}$ concentration also did not change much throughout the day with mean concentrations for the altitude-varying flights of 35.1, 37.2, and 36.8 μg/m^3. The flight flown at a constant altitude had a lower concentration of 23.5 μg/m^3. This reduction in concentration is much larger than the concentration variation in any of the first three flights, and therefore, the constant altitude most likely does not account for the change; however, more data are needed to draw any conclusions on the cause of the change.

To characterize variation on the satellite data subpixel scale, the fourth flight was conducted at a near-constant altitude of 60 m. Data were then sectioned into a 120 m × 65 m grid. The mean $PM_{2.5}$ concentration across the grid cells ranged from 20.5 to 24.9 μg/m^3. This range is within the standard deviation of any grid cell. Thus, a data pixel with an area equivalent to the flight path area would accurately characterize the PM concentration of this region.

This system has proven to be qualified to gather the measurements needed for proper validation of satellite observations and data products. With the continued drop in cost and sensor size, this proof of concept could easily transition into multiple vehicles used on a routine basis to help validate all future missions.

Acknowledgments

The views expressed in this paper are those of the authors and do not necessarily represent the views of NASA. The authors would also like to thank David Schaefer for piloting their aircraft throughout this study.

Author Contributions

Conceived and designed the experiments: WAH. Analyzed the data: WAH, AGM. Wrote the first draft of the manuscript: WAH. Contributed to the writing of the manuscript: WAH, BJN. Agree with manuscript results and conclusions: WAH, DJL, BJN. Jointly developed the structure and arguments for the paper: WAH, DJL. Made critical revisions and approved final version: WAH, DJL, BJN. All authors reviewed and approved of the final manuscript.

REFERENCES

1. Haywood J, Boucher O. Estimates of the direct and indirect radiative forcing due to tropospheric aerosols: a review. *Rev Geophys*. 2000;38(4):513–543.
2. Lohmann U, Feichter J. Global indirect aerosol effects: a review. *Atmos Chem Phys*. 2005;5(3):715–737.
3. Lohmann U. A glaciation indirect aerosol effect caused by soot aerosols. *Geophys Res Lett*. 2002;29(4):1052.
4. Wang W, Domoto G. The radiative effect of aerosols in the earth's atmosphere. *J Appl Meteorol*. 1974;13:521–534.
5. Warren SG, Wiscombe WJ. A Model for the spectral albedo of snow II: snow containing atmospheric aerosols. *J Atmos Sci*. 1980;37(12):2734–2745.
6. Chylek P, Wong J. Effect of absorbing aerosols on global radiation budget. *Geophys Res Lett*. 1995;22(8):929–931.
7. Brook RD, Rajagopalan S, Pope I, et al; Amer Heart Assoc Council, D. Council Kidney Cardiovasc, and M. Council Nutr Phys Activity. Particulate matter air pollution and cardiovascular disease an update to the scientific statement from the American Heart Association. *Circulation*. 2010;121(21):2331–2378.
8. Brook RD, Bard RL, Kaplan MJ, et al. The effect of acute exposure to coarse particulate matter air pollution in a rural location on circulating endothelial progenitor cells: results from a randomized controlled study. *Inhal Toxicol*. 2013;25(10):587–592.
9. Brook RD, Xu X, Bard RL, et al. Reduced metabolic insulin sensitivity following sub-acute exposures to low levels of ambient fine particulate matter air pollution. *Sci Total Environ*. 2013;448:66–71.
10. Pope I, Arden C, Brook RD, Burnett RT, Dockery DW. How is cardiovascular disease mortality risk affected by duration and intensity of fine particulate matter exposure? An integration of the epidemiologic evidence. *Air Qual Atmos Health*. 2011;4(1):5–14.
11. Ballester F, Medina S, Boldo E, et al. Reducing ambient levels of fine particulates could substantially improve health: a mortality impact assessment for 26 European cities. *J Epidemiol Community Health*. 2008;62(2):98–105.
12. Boldo E, Medina S, LeTertre A, et al. Apheis: health impact assessment of long-term exposure to pm2.5 in 23 European cities. *Eur J Epidemiol*. 2006;21(6):449–458.
13. Boldo E, Linares C, Lumbreras J, et al. Health impact assessment of a reduction in ambient pm2.5 levels in Spain. *Environ Int*. 2011;37(2):342–348.
14. Dockery DW, Pope CA, Xu XP, et al. An association between air-pollution and mortality in 6 United States cities. *New Engl J Med*. 1993;329(24):1753–1759.
15. Ginoux P, Torres O. Empirical TOMS index for dust aerosol: applications to model validation and source characterization. *J Geophys Res Atmos*. 2003;108(D17).
16. Prospero JM. Global dust transport over the oceans: the link to climate. *Geochim Cosmochim Acta*. 2003;67(18):A384–A384.
17. Harrison WA, Lary D, Nathan B, Moore AG. The neighborhood scale variability of airborne particulates. *J Environ Prot*. 2015;6(5):464–476.
18. Nance JD, Hobbs PV, Radkel LF. Airborne measurements of gases and particles from an Alaskan wildfire. *J Geophys Res Atmos*. 1993;98(D8):873–882.
19. Novakov T, Hegg DA, Hobbs PV. Airborne measurements of carbonaceous aerosols on the East Coast of the United States. *J Geophys Res Atmos*. 1997;102(D25):30023–30030.
20. Orsini DA, Ma Y, Sullivan A, Sierau B, Baumann K, Weber RJ. Refinements to the particle-into-liquid sampler (PILS) for ground and airborne measurements of water soluble aerosol composition. *Atmos Environ*. 2003;37(9):1243–1259.
21. Huntrieser H. Intercontinental air pollution transport from North America to Europe: experimental evidence from airborne measurements and surface observations. *J Geophys Res*. 2005;110(D01305):1–22.
22. Sullivan AP, Peltier RE, Brock CA, et al. Airborne measurements of carbonaceous aerosol soluble in water over northeastern United States: method development and an investigation into water-soluble organic carbon sources. *J Geophys Res Atmos*. 2006;111(D23S46):1–14.
23. Loughner CP, Lary DJ, Sparling LC, Cohen RC, DeCola P, Stockwell WR. A method to determine the spatial resolution required to observe air quality from space. *IEEE Trans Geosci Remote Sens*. 2007;45(5):1308–1313.
24. Weinzierl B, Petzold A, Esselborn M, et al. Airborne measurements of dust layer properties, particle size distribution and mixing state of Saharan dust during SAMUM 2006. *Tellus B Chem Phys Meteorol*. 2009;61(1):96–117.

25. Maletto A, McKendry I, Strawbridge K. Profiles of particulate matter size distributions using a balloon-borne lightweight aerosol spectrometer in the planetary boundary layer. *Atmos Environ*. 2003;37(5):661–670.
26. McKendry IG, Sturman AP, Vergeiner J. Vertical profiles of particulate matter size distributions during winter domestic burning in Christchurch, New Zealand. *Atmos Environ*. 2004;38(29):4805–4813.
27. Aurell J, Gullett BK. Emission factors from aerial and ground measurements of field and laboratory forest burns in the southeastern us: Pm2. 5, black and brown carbon, voc, and pcdd/pcdf. *Environ Sci Technol*. 2013;47(15):8443–8452.
28. Aurell J, Gullett BK. Aerostat sampling of pcdd/pcdf emissions from the Gulf oil spill in situ burns. *Environ Sci Technol*. 2010;44(24):9431–9437.
29. NASA. 2013. Available at: decadal.gsfc.nasa.gov
30. MicroPilot. 2014. Available at: www.micropilot.com
31. Draxler RR, Hess G. An overview of the HYSPLIT 4 modelling system for trajectories, dispersion and deposition. *Aust Meteorol Mag*. 1998;47(4):295–308.